

See discussions, stats, and author profiles for this publication at: <https://www.researchgate.net/publication/361271848>

Resonator-based Pressure Sensor for Wall Pressure

Conference Paper · June 2022

DOI: 10.2514/6.2022-2956

CITATIONS

2

READS

155

10 authors, including:



Shishir Damani

Virginia Tech (Virginia Polytechnic Institute and State University)

8 PUBLICATIONS 16 CITATIONS

SEE PROFILE



Máté Szőke

Blue Ridge Research and Consulting (BRR)

53 PUBLICATIONS 696 CITATIONS

SEE PROFILE



William Devenport

Virginia Tech (Virginia Polytechnic Institute and State University)

335 PUBLICATIONS 5,349 CITATIONS

SEE PROFILE



N. Agastya Balantrapu

University of Utah

13 PUBLICATIONS 63 CITATIONS

SEE PROFILE



Resonator-Based Pressure Sensor for Wall Pressure

Shishir Damani, Erik Braaten*, Máté Szóke†, Nathan Alexander ‡ and William J. Devenport§
Virginia Polytechnic Institute and State University, Blacksburg, Virginia 24061, United States of America

N. Agastya Balantrapu¶
Princeton University, Princeton, New Jersey 08544, United States of America

Benjamin P. Pearce||, Timothy A. Starkey**, Alastair P. Hibbins††, J. Roy Sambles‡‡
University of Exeter, Exeter, Devon EX4 4QL, United Kingdom

A Kevlar-covered acoustic resonator-based cavity sensor is introduced to measure low-wavenumber pressure fluctuations in a turbulent boundary layer. These sensors have an inherent capability to filter the convective pressure fluctuations based on their physical dimensions, specifically their extent in the streamwise and spanwise directions. This study aims to demonstrate the spatial sensitivity behavior of these sensors and to show their viability towards wall pressure measurements by revealing the lack of effects on the turbulent flow over a sensor using a time-resolved wall parallel flow visualization technique. Additionally, it examines the degree of control that can be achieved on the spatial response of such sensors using sensor shape, and flow interfaces with different materials and porosity distributions. Understanding the sensor operation in this way may enable these sensors to be used more widely.

Nomenclature

| | | |
|------------------|---|---|
| p | = | Pressure fluctuation |
| ρ | = | Fluid density |
| x_i | = | Position along i^{th} direction |
| U_i | = | Mean velocity in i^{th} direction |
| δ | = | Boundary layer thickness |
| f | = | Frequency |
| k_3 | = | Wavenumber in spanwise direction |
| u_i | = | Velocity fluctuation in i^{th} direction |
| $\overline{u_i}$ | = | Mean of velocity fluctuation in i^{th} direction |
| U_m | = | Maximum velocity of boundary layer in stream/flow direction |
| ν | = | Kinematic viscosity |
| u_τ | = | Friction velocity in stream/flow direction |
| Re_τ | = | Friction Reynolds number |
| G_{uu} | = | Autospectrum of quantity u_1 |
| $\sqrt{u_i^2}$ | = | Reynolds stress in i^{th} direction |
| CR | = | Sensor Dynamic Response Function |

*Graduate Research Assistant, Kevin T. Crofton Dept. Aerospace & Ocean Engineering, and AIAA Student Member

†Senior Research Associate, Kevin T. Crofton Dept. Aerospace & Ocean Engineering, and AIAA Member

‡Assistant Professor, Kevin T. Crofton Dept. Aerospace & Ocean Engineering, and Senior Member AIAA

§Crofton Professor of Engineering, Kevin T. Crofton Dept. Aerospace & Ocean Engineering, and AIAA Fellow

¶Postdoctoral Research Associate, Dept. of Mechanical and Aerospace Engineering, AIAA Member

||Ph.D. Student, Department of Physics and Astronomy

**Research Fellow, Department of Physics and Astronomy

††Professor, Department of Physics and Astronomy

‡‡Professor, Department of Physics and Astronomy

I. Introduction

TURBULENT boundary layer flows have a large range of temporal and spatial scales and structures which can be studied mainly in two ways: (a) the velocity field, and (b) the pressure fluctuations impinging on the surface over which the flow occurs. These are coupled by the Pressure Poisson equation which is a theoretical description of the flow physics (derived from the momentum equation) and is given by:

$$\frac{1}{\rho} \nabla^2 p = -2 \frac{\partial U_i}{\partial x_j} \frac{\partial u_j}{\partial x_i} - \frac{\partial^2}{\partial x_j \partial x_i} (u_i u_j - \overline{u_i u_j}) \quad (1)$$

The first term on the right is referred to as the rapid, or linear, term and captures the direct mean flow changes while the second term is the slow, or non-linear, term responding to the indirect changes from the mean flow due to non-linear interactions. This equation can be integrated over the flow volume to yield the wall pressure at any location on the surface. Due to the presence of non-linear terms, the equation does not have any analytical solution except for some special scenarios, and hence this is where measurements using surface pressure transducers/sensors or microphones are useful. Boundary layer pressure fluctuations are largely broadband and are contributed by a variety of three-dimensional flow structures. Often the surface pressure fluctuations are decomposed into the frequency and wavenumber domain to study the contribution from various scales. This decomposition is relatively straightforward in the case of two-dimensional homogeneous boundary layer flows where the wall pressure wavenumber frequency spectrum is the Fourier transform of the two-point space-time correlation of the surface pressure fluctuation $R_{pp}(\vec{x}, \vec{x}', \tau)$. This correlation function can be obtained using a pair of pressure sensors separated in space where the sensors are mounted flush on the surface of interest to avoid any significant flow disruptions. There have been numerous studies documenting the behavior of the wavenumber-frequency spectrum or the space-time correlation. These studies have classified the wavenumber-frequency spectrum into several regions namely acoustic/supersonic, sub-convective, and convective regions. Among these studies many have shown that the convective region is the most dominant and the contributions in this region are due to structures convecting with the flow [1, 2]. In particular, Willmarth *et al.*[1] showed space-time correlation measurements parallel to the stream direction to have maxima at certain time delays corresponding to the convection of flow structures with a speed 60-80% of the stream speed.

Arrays of microphones have helped identify contribution from structures apart from the convective scales, presumably due to elongated or large-scale structures which couple to the flow surface, or even acoustic noise. Graham *et al.*[3] showed a coupling between boundary layer pressure fluctuations and the structural vibration modes of the surface/panel over which the flow occurred to be a significant contributor to the far-field sound spectrum. A change in the physical properties of the structure including its boundary condition and/or bulk properties affected the far-field spectrum predictions significantly. The convective pressure fluctuations were separated as the hydrodynamic coincident part by identifying the resonant frequencies obeying the convective speed relation. However, it was noticed that apart from the resonant modes, which dominated the levels, there were other modes corresponding to the structural modes of the panel itself which were more efficient in radiating sound when coupled with the excitation source. This highlighted the importance of sub-convective structures of the order of the panel size and these were identified to be responsible for panel vibrations in turn interior noise. Usually, the flow structures contributing to the weak pressure fluctuations are masked by the convective and acoustic contamination and these are large in scale as these fall under the sub-convective domain.

There have been various studies to quantify the contribution of these sub-convective structures in boundary layer flows involving the use of at least three techniques. Firstly, 'small array/large sensors' were used to filter out small-scale/dominant fluctuations associated with the convective motions but these are limited in spatial resolution due to their size and suffered from inherent aliasing [4, 5]. Secondly, 'membranes/thin-walled sheets' were used to measure the large structures by studying the mode shapes of the membranes and identifying their coupling with the pressure fluctuations [3, 6, 7]. Thirdly, 'large array/small sensors' were used to resolve the convective scales effectively but suffered from poor signal-to-noise ratio for the weaker structures [8, 9]. These three approaches have yielded some idea of the sub-convective domain, however there is a disagreement between experimental measurements and model predictions (see Figure 2.36 in [10] and Figure 6/7 in [11]). A major reason for this is the difficulty in matching experimental conditions, and assumptions to simplify the models. Graham *et al.*[11] and Blake [10] show a comparison between various models and highlight the discrepancies among the existing models. Additionally, the use of pressure sensitive paints (PSPs) has increased due to their high resolution. However, their use in low speed flows is still limited due to the sensitivity of the paint to weak pressure fluctuations and temperature-induced errors [12]. This suggests that the pressure sensing methods available have limitations especially in terms of spatial aliasing and poor signal-to-noise ratios making it challenging to measure the weaker pressure fluctuations in the boundary layer.

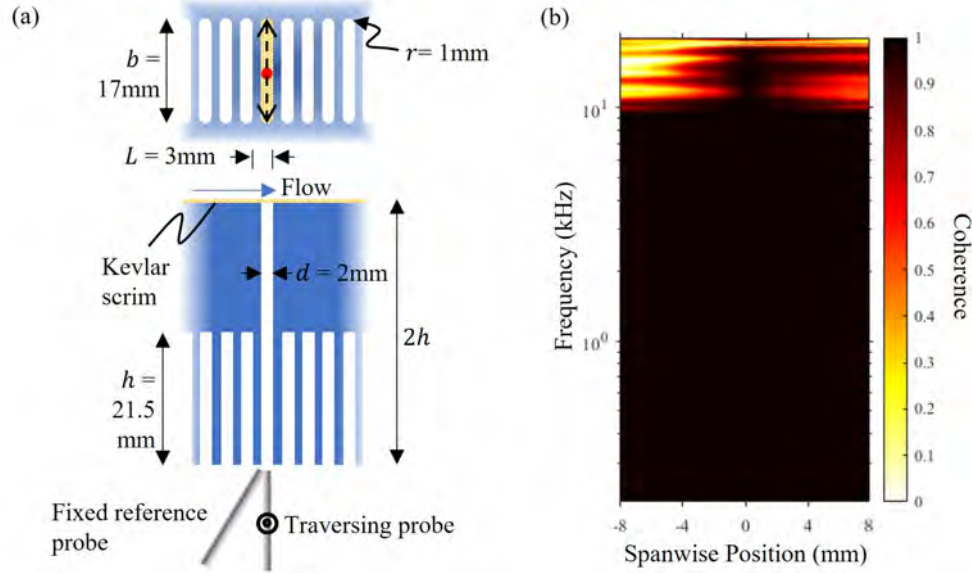


Fig. 1 (a) Schematic of a pressure field scan under a metasurface excited by a turbulent flow; Top: underside, Bottom: cut-through cross-section, (b) Spanwise coherence of the half-wave cavity [13]

Recently, in a study of acoustic metasurfaces excited by turbulent flow, Damani *et al.* [13], discovered that resonant cavities might have desirable properties for sensing larger scale pressure fluctuations. The metasurface was connected to the turbulent flow through a half wave cavity in the flow surface (Figure 1(a)), the flow side of which was covered by Kevlar cloth to avoid significant disturbance to the flow. They found that, despite the fine structure of much of the instantaneous pressure field associated with convecting structures, pressure fluctuations measured at the lower open end of the half-wave cavity were almost perfectly coherent and in phase across the resonator cross section. Using cross-correlation between two microphones, one fixed at the center of the half-cavity and second traversed the length of the half-wave cavity as depicted in Figure 1(a), a coherence map was shown (Figure 1(b)). This map shows the frequency in Hertz on the y - axis and the location of the traversing microphone on the x - axis in millimeters with 0 representing the location of the fixed microphone at the center of the cavity. The map shows perfect coherence (color scale of 1) until about 10 kHz beyond which the coherence drops as we approach the ends of the half-wave cavity. This was observed due to effects of cross-modes sitting across the length of the cavity at high frequencies. Here the cross-mode was at 10 kHz for a cavity of length 18 mm. Ensuing from Damani *et al.*[13], the idea to use Kevlar-covered quarter-wave cavities as sensors was logical. This allowed a pressure transducer to be installed at the closed-end of the cavity and avoid any contamination due to radiation from the surrounding when it was open. Fundamentally, this would change the resonant modes of the cavity but, it might also affect the uniform pressure field behavior.

Figure 2 shows the basic concept of the sensor. The components can be identified as an acoustic resonating cavity, a flow interface usually a Kevlar scrim or a thin metal sheet with pores and a microphone. The flow interface is intended to act as an acoustically transparent layer between the turbulent flow and the pressure field inside the cavity which allows the transmission of pressure fluctuations but prevents any measurable flow disruptions. The profile of a sensor is defined by a horizontal cross-section of the sensor which is a rectangle for Figure 2. These sensors are simple to construct in a wide variety of forms using rapid prototyping and inexpensive microphone transducers. This type of sensor was used in a recent study by Damani *et al.*[14] where quarter-wave cavities of rectangular profile housing a microphone at the closed bottom were used to measure low-wavenumber pressure fluctuations in zero pressure gradient turbulent boundary layer flows over smooth walls. The cavity was covered with a Kevlar scrim to transmit the pressure fluctuations without disturbing the flow. The sensor length chosen was of the order of the boundary layer thickness to spatially filter convective pressure fluctuations on the order of the boundary layer thickness and the sensors were arranged in the direction of the flow to minimize aliasing by having overlapping sensors with least possible separation across the flow. The sensor helped address two main issues in low-wavenumber measurements i.e., spatial aliasing and low signal-to-noise ratios due to convective fluctuations dominance. However, a key assumption of Damani *et al.*[14] was that the pressure field at the bottom a quarter-wave cavity sensor was coherent and that the sensor exhibited uniform

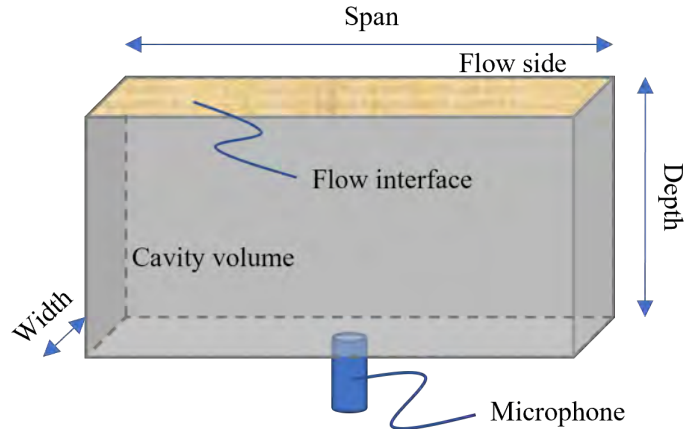


Fig. 2 Schematic of a resonator-based sensor

area sensitivity over its surface. This raised several questions about the potential of resonator-based sensors. The overarching goal of the research described in this paper is to investigate these assumptions and possibilities, specifically:

- 1) To establish the coherence of the pressure field generated at the base of quarter wave resonating sensors of different design,
- 2) To understand the effects of cavity shape on its dynamic behavior,
- 3) To measure the actual spatial sensitivity distribution of this type of sensor,
- 4) To quantify any effects of a Kevlar-covered resonating cavity sensor on boundary layer flow over the region of the sensor, and
- 5) To determine the degree of dependence of the dynamic response of the sensor response on the flow interface, especially segregating effects of material modal response and porosity.

To attain these goals aerodynamic and acoustic measurements have been made on a range of resonating sensor designs. The designs are described in section II. In section III we present results of studies on the dynamic response functions, the spatial sensitivity function, the disturbance produced by a wall-mounted sensor, and the effects of changes in the flow interface of the sensor on its response. Overall, we find that Kevlar-covered resonating sensors have almost no influence on an over-riding flow, have almost uniform spatial sensitivity distribution, can have any profile shape although their response would be limited by the first mode across their length and that the pressure excitation from the flow is mediated only by pores in the flow interface. The proposed sensors appear useful in designing arrays with new capabilities, namely, measuring low-wavenumber pressure fluctuations in boundary layer with higher wavenumber resolution and significantly reduced aliasing, and also possibly detecting acoustic sources through the boundary layer.

II. Resonator-Based Sensors Studied

In order to meet the above goals, experiments were performed on a series of 13 resonating sensors of differing configurations including the profile shape and the flow interface. These sensors used quarter-wave resonating cavities produced using rapid prototyping SLA technology on a Connex 3 printer with ABS plus material. The layer thickness of this printer was 16 microns producing fairly smooth surfaces on the insides of the cavity. Table 1 lists the different sensor configurations with shape profiles and flow interfaces tested. Here, the shape profile of a slot refers to a rectangle of span 15 mm with semicircles of radius 1.5 mm at each end while the mirrored Hanning refers to a Hanning window function of height half the sensor width i.e., 1.5 mm mirrored about its base. A wall thickness of 5 mm was found to be sufficient to suppress any significant coupling with pressure fluctuations inside the cavity.

Each printed cavity was part of an insert which mounted onto a 609.6 mm \times 609.6 mm aluminum plate such that it was flush on one side of the plate. The plate formed part of the test wall of the VT Anechoic Wall Jet Facility [13, 15] in which all measurements, with and without flow, were performed. The edges of the insert were taped to the plate using a 40 micron tape for minimum diffraction and disturbance to flow. As indicated in Table 1, a series of different flow interfaces/membranes were used with the resonating cavities, including rigid sheet metal and different OAR Kevlar scrim. The membrane properties can be found in detail in section III.E.

Kevlar scrim was applied over the cavity using spray adhesive while the rigid material membranes used a double sided tape ensuring no gaps. Metal membranes were studied in order to reveal a comparison between flexible fabric scrims and rigid membranes made of sheet metal. This would also open up the domain of studying effects of different porosity distributions and possibly having distributions for specific sensor dynamic response. A few tests were performed with no membrane installed at all, for reference. A Brüel & Kjær Type 4182 with a 25 mm probe tip was used to measure the pressure fluctuations at the bottom of the cavity, ensuring no leaks. The tip of the microphone was made flush with the inner surface of the cavity by using a limiter knob on the probe tip.

| Sensor Type | Profile | Dimensions in mm (Span/Width/Depth) | Flow Interface (Thickness in mm) | OAR(%) |
|-------------|------------------|--|-------------------------------------|--------|
| A | Slot | 18/3/21 | None | 100 |
| B | Slot | 18/3/21 | Kevlar 120 (0.08) | 2 |
| C | Rectangle | 18/3/21 | Kevlar 120 (0.08) | 2 |
| D | Rectangle | 50/3/21 | Kevlar 120 (0.08) | 2 |
| E | Mirrored Hanning | 18/3/21 | Kevlar 120 (0.08) | 2 |
| F | Slot | 18/3/42 | Kevlar 120 (0.08) | 2 |
| G | Slot | 18/3/21 | 6061 Aluminum (0.508) | 0 |
| H | Slot | 18/3/21 | 6061 Aluminum (0.508) | 6.6 |
| I | Slot | 18/3/21 | 6061 Aluminum (0.406) | 6.6 |
| J | Slot | 18/3/21 | 6061 Aluminum (0.508) | 3.3 |
| K | Slot | 18/3/21 | 6061 Aluminum (0.508) | 3.3* |
| L | Slot | 18/3/21 | Kevlar (0.08) | 0.01 |
| M | Slot | 18/3/21 | Kevlar (0.08) | 6 |

Table 1 Table of different sensor configurations studied. * refers to a different porosity distribution

III. Results and Discussions

Following from the objectives of this study, this section is divided into four sub-sections. In section III.A, we present measurements demonstrating the dynamic relationship between a uniform pressure experienced at the top of a Kevlar-covered cavity and those recorded at a microphone placed at the bottom of the resonating cavity. We examine the sensor dynamic response for sensor types A through E in order to establish that a quarter-wave cavity has a coherent pressure field and to observe the effects of profile shape. Section III.B also show measurements of the coherence of the pressure field at the bottom of sensor B and E. In section III.C we present and discuss detailed measurements made using a highly local monopole source traversed over the top of the membrane of sensor D. The purpose of these measurements is to establish the spatial sensitivity functions associated with these membrane/resonator combinations, in particular a Kevlar-covered resonator. Section III.D is focused on quantifying the effects of a Kevlar-covered cavity on a turbulent wall-jet boundary layer flow. This uses a different sensor configuration involving a half-wave cavity instead of a quarter-wave cavity. This was considered a more stringent test as an open-open cavity may effect the boundary layer flow more than a cavity closed at the bottom. Lastly, section III.E studies the effects of flow interface on the sensor dynamic response from the perspective of flexibility of material and porosity. This is mainly done to determine the driving factor of the sensor dynamic response if the membrane is changed. Depending on the result, membranes could be manufactured to yield desirable characteristic. Each section describes the experimental setup and the corresponding results targeting the objectives of this study.

A. Sensor Dynamic Response Measurement

An experiment was devised to measure the sensor dynamic response, i.e. the transfer function between uniform pressure fluctuations experienced on the top of the sensor membrane, and that recorded by the transducer in its base. To do this a white noise source (Visaton FRS8-8 Ohm speaker) was placed 30" above the sensor (Figure 3) aligned with the

center of the sensor profile. Cross-spectra with the source and a probe microphone (B&K Type 4182 with 25 mm probe tip) placed at the flow surface, adjacent to the flow interface, and at the base of each sensor resonator were measured. The dynamic response function of each sensor was determined as the ratio of these spectra. Data were sampled at a frequency of 65536 Hz for a duration of 32 seconds and the spectra calculations were performed using 8192 samples with 50% overlap giving a total of 511 averages.

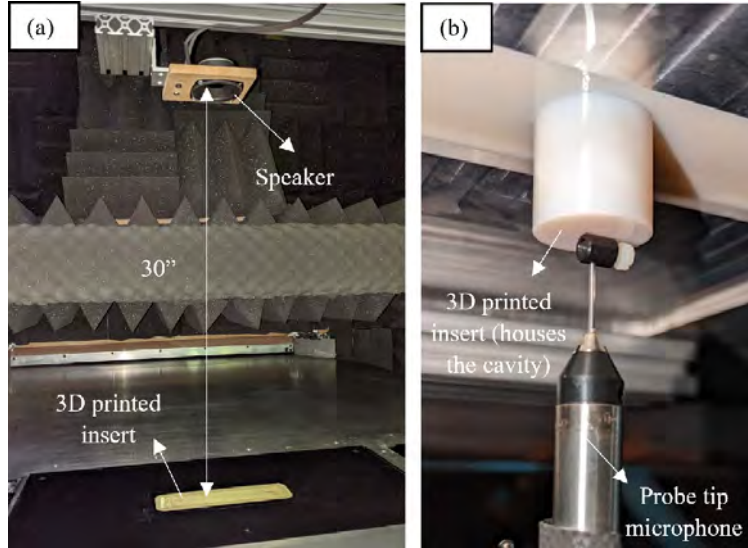


Fig. 3 Photographic view of setup for measuring the sensor dynamic response (a) Speaker side, (b) Cavity side

Figure 4 shows results for sensors A through E all 18 mm wide sensors along with their profile shape. Sensors B-E, were covered with a Kevlar 120 scrim (0.08 mm thick, a thread density of 34 filaments per inch in both directions with 2% OAR). Sensor A is the reference for this set with a slot profile and no Kevlar interface. The sensor dynamic response function for each configuration is depicted in Figure 4 and these have been 12^{th} octave binned. The blue curve

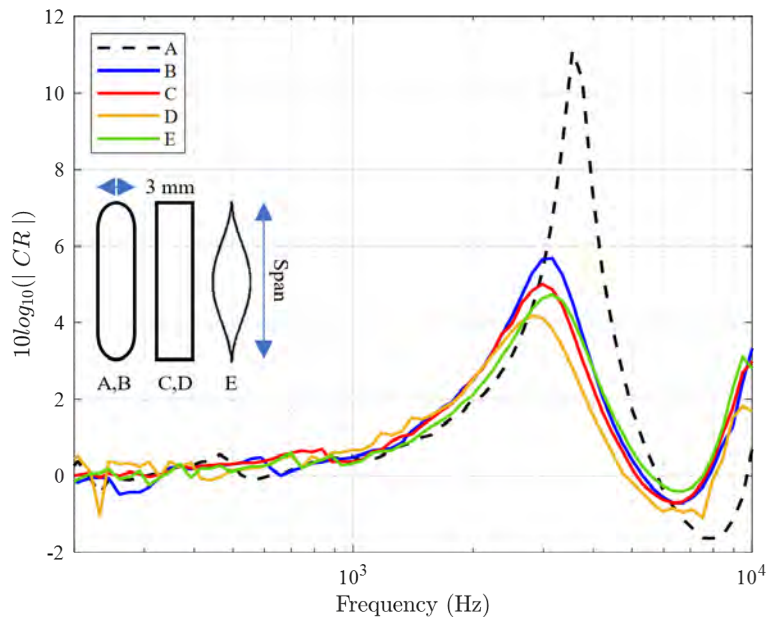


Fig. 4 Sensor dynamic response function showing the effects of profile shape

represents the slot, the red a rectangle and the green is the mirrored Hanning profile, all spanning a length of 18 mm, width of 3 mm and a depth of 21 mm. Sensor E has a rectangular profile with a length of 50 mm but the same width and depth as the others. The low frequency variation lies within the uncertainty limits of ± 0.8 dB. The resonant depth mode of the reference sensor A is realised to be at about 3.6 kHz (first peak) which is close to the theoretical quarter-wave mode of 4 kHz while the Kevlar-covered sensors observe a drop in the modal frequency response to about 3 kHz for the first mode due to a change in the impedance boundary condition owing to the presence of a Kevlar scrim as well as due to end-effects. There is a striking resemblance of the sensor dynamic response function for various Kevlar interfaced shapes tested and this is due to the same depth resonance characteristics. This suggests no major effects of the profile shape on the sensor dynamic response however, this conclusion would be misleading without considering the spanwise coherence of such shapes.

B. The Coherence of the Pressure at the Sensor Base

It is also important to quantify any changes to the spanwise uniformity behavior with a change in shape as a loss in coherence would imply an impractical sensor characteristic. The coherence at the bottom of the sensor was tested for a sensor B and E by taking pressure measurements at various points along the span of the cavity using two probe tip microphones at the base of the sensor. One microphone was fixed at the center span of the sensor while the other traversed along the span. Specific span locations (indicated in results) were chosen and for each measurements the other holes for the microphone were blocked. These measurements were conducted in the Anechoic Wall Jet Facility [13] with fully developed turbulent flow exciting the Kevlar-covered sensors. The boundary layer properties just above the sensor were $\delta = 13.3$ mm and $U_m = 24$ m/s. The coherence maps for both the sensors are shown in Figure 5. The abscissa corresponds to the location along the length of the slot in millimeters and the ordinate shows the frequency in kHz on a logarithmic scale. Sensor B (Figure 5(a)) shows a perfect coherence (color scale of 1) along the length of the cavity until about 14 kHz which corresponds to the fundamental mode along the span of the cavity. Beyond this mode, cross modes exist in the cavity which give rise to a non-uniform behavior as you move away from the center of the cavity. Coherence is not much of value if there is no phase relation between the two microphones, hence Figure 5(a) also plots the unwrapped phase between the microphones indicating no phase difference which hints to a uniform pressure field at the bottom of the cavity despite a stochastic excitation over the top. Similarly, sensor E observes a perfect coherence region shifted up in frequency compared to the sensor B (Figure 5(b)) despite the same span. This is suspected to be due to an effective change in length of the Hanning cavity due to support material blockage at the converging ends.

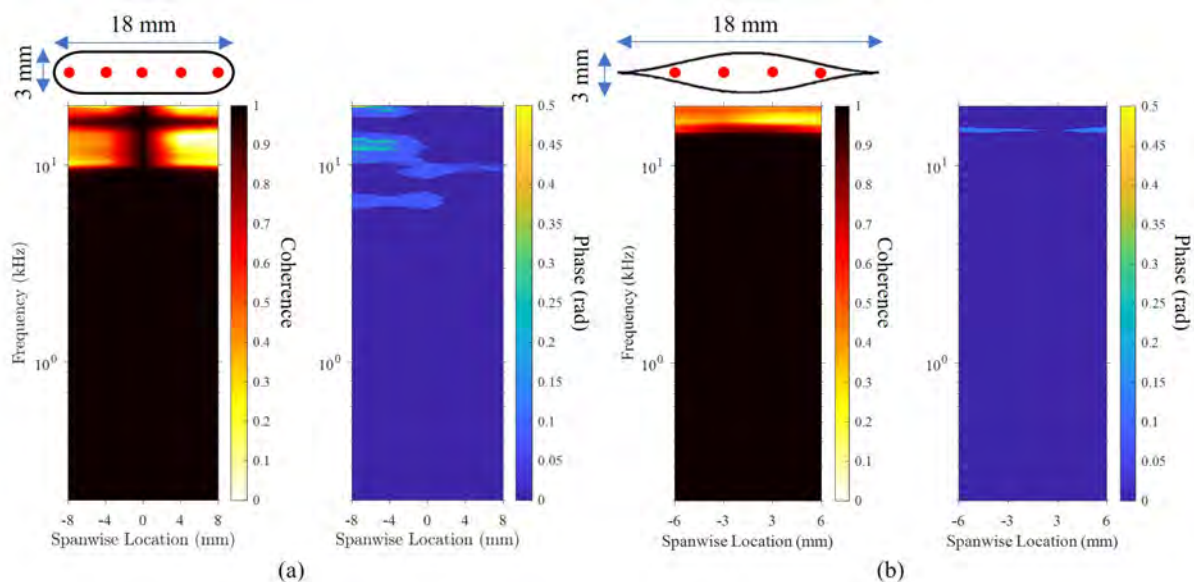


Fig. 5 Spanwise coherence and phase contour for (a) Sensor B, (b) Sensor E when excited using turbulent flow. The location of traversing microphone is shown with respect to the sensor profile

C. Spatial Sensitivity Function Measurement

The spanwise coherence at the sensor bases observed in section III.B does not imply a uniform spatial sensitivity function of the sensor. Using a localized sound field, the area-sensitivity function of the sensors could be measured. An experimental setup was designed involving a source of monopole nature. A KOSS Sparkplug earphone (operating frequency range of 16 - 20000 Hz) was used as a source due to its localized sound field. The source was supported using a low profile rod to minimize diffraction. It was very important to establish that the source had a monopole character implying that the sound coming from the earphone tip dominated the sound from the earphone housing. This was indeed found to be true for this earphone speaker arrangement (Figure 6). The source behaved as a monopole within ± 3 dB for frequencies between 400 and 9000 Hz.

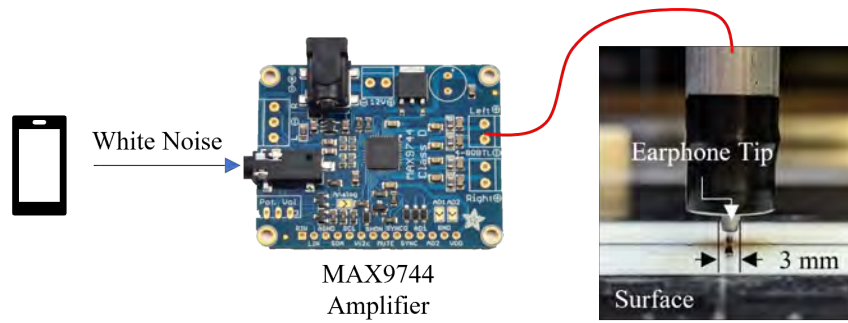


Fig. 6 A schematic of the localized sound field speaker arrangement.

Using this speaker arrangement, the spatial sensitivity was tested by measuring the sound field using sensor type D in Table 1. The sensor was 50 mm in length, 3 mm wide and 21 mm deep which corresponded to a span mode of 3.4 kHz and a depth mode of 4 kHz without a Kevlar interface. The procedure of measurement was similar to the sensor dynamic response measurement except that the source was traversed over the sensor staying at a height of 2 mm over the surface. Seven different locations were chosen over the sensor domain such that 5 were over the sensor profile while two were beyond the profile dimensions. A schematic of the setup is shown in Figure 7(a) with a single source location over the center of the sensor along with the microphone location. Figure 7(b) shows a photograph of the source over the Kevlar-covered sensor. For each of the excitation location, the probe microphone measurements were taken at the center of the quarter-wave cavity as in Figure 7(a). To investigate the spatial sensitivity, change in sensor dynamic response is studied which would reflect the spatial averaging performed by the sensor with different source locations depending on its spatial sensitivity. This implies that a uniform spatial sensitivity would have no changes in the dynamic response function.

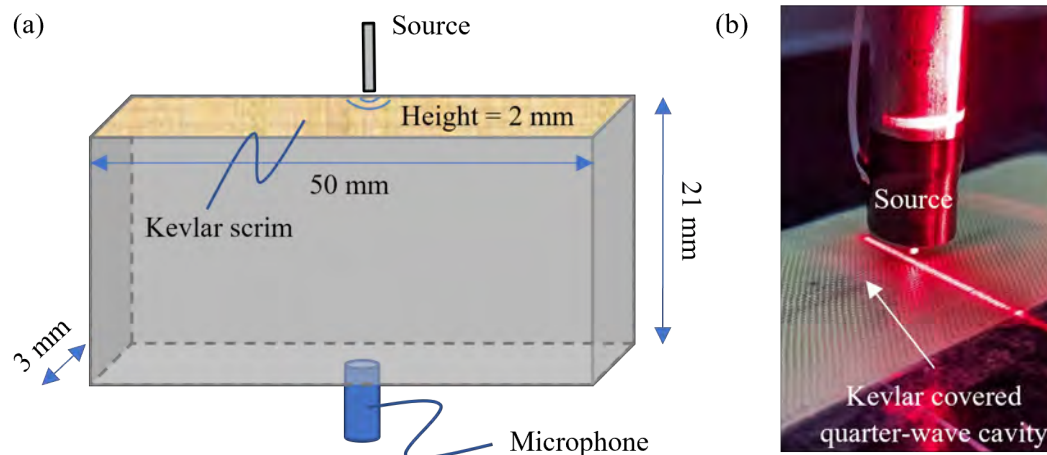


Fig. 7 Area sensitivity measurement setup: (a) Schematic (b) Photograph of the top side of the Kevlar interfaced cavity showing the source.

A schematic of source locations and the sensor dynamic response of the sensor is shown in Figure 8. The sensor dynamic response has been normalized on spatially averaged pressure amplitude, assuming an ideal monopole source over a surface. The ideal monopole was modeled using a volumetric source equation based on same locations of the source over the cavity as were tested experimentally. A two-dimensional domain was chosen slightly larger than the cavity dimensions and an integration of the pressure amplitude over the cavity region was obtained. The difference between the integrated pressure amplitude for the case of when the source is over the center of the cavity and when it is at other locations is calculated and divided out from the measured data. It can be observed that the plots collapse onto one another as the difference in spatially averaged levels is accounted by the normalization. Note that the microphone was located at the bottom center of the cavity for all measurements and only the source location was changed. The behavior of the response functions lies within the uncertainty band of ± 0.8 dB for all source locations until a frequency of approximately 3.4 kHz, beyond which the results deviate. The locations equidistant with respect to the center of the cavity seem to have similar trend consistent with the symmetric nature of the sound field. The first peak corresponds to the resonant mode of the cavity which is lower than the theoretical mode due to absence of a Kevlar interface. These results demonstrate that the Kevlar interfaced cavity has an almost constant spatial sensitivity and thus averages the pressure over its surface.

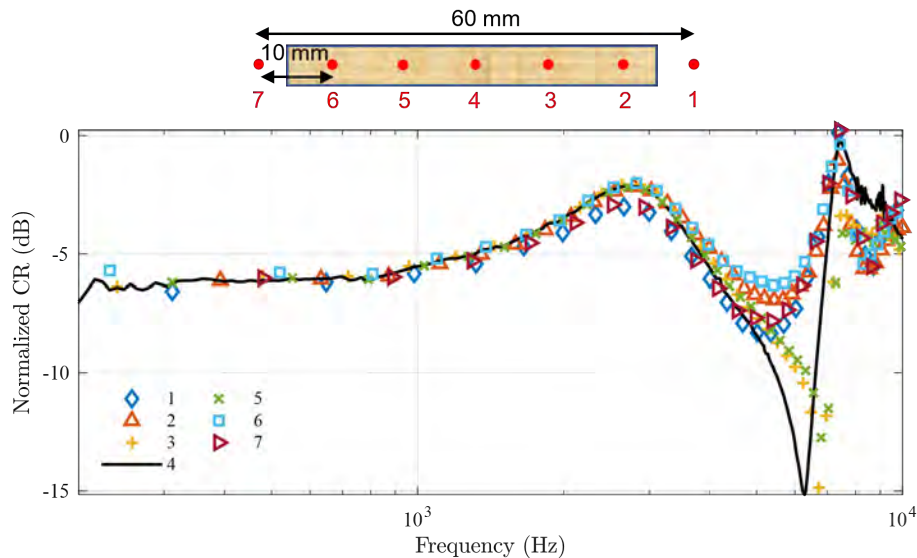


Fig. 8 Sensor dynamic response function for sensor type D when excited by a point source over its surface at different locations.

D. Flow Disturbance Quantification

To assess any potential interaction between the flow and the cavity, the flow around the cavity opening was captured using a two-dimensional high-speed particle-image velocimetry (PIV) system. This study was performed in the Anechoic Wall Jet Facility at Virginia Tech which has been described in detail in Damani *et al.*[13]. A fully developed wall jet boundary layer is formed on a large plate which comprises of a 609.6 mm \times 609.6 mm provision for the sensor panel. The flow has been very well characterized by Kleinfelter *et al.*[15].

Flow interference measurements were made using sensor F, which is a 42 mm deep half-wave cavity (open lower end) with a slot-shaped profile 18 mm by 3 mm, covered with 2% open area ratio Kevlar 120 scrim. For the flow test the sensor was placed with its long axis spanwise across the flow. The Kevlar covering formed a rectangular patch that extended ± 25.4 mm from the center of the sensor in spanwise and streamwise directions. To examine this in detail we consider a wall-parallel cross-section of the flow located 1.25 mm from the surface and measured using planar PIV. The region of study is 75 mm in the flow direction (x_1) and 46.5 mm across the flow direction (x_3). Measurements were made both of the flow over the sensor and the flow over a plain wall with the sensor removed. The entire Kevlar interfaced cavity was part of the flow field and its location is highlighted in the results discussed.

The PIV system consisted of a Phantom v2512 high-speed camera (1280 \times 800 pixels), a Photonics DM150-532

high-speed laser, and a LaVision high-speed controller. Seeding was introduced to the flow at the suction side of the wind tunnel fan using an MDG MAX300APS type fog generator. A 200 mm/f2 Nikon lens was used at an aperture of f5.6 to enable a detailed analysis of the flow field. The distance between the front lens and the laser sheet was 1.2 m, resulting in a field of view (FOV) size of 100×70 mm and a fine spatial resolution of 13.13 pixel/mm [16]. For image calibration, pinhole camera model calculations and a LaVision type 106-10 calibration plate were used. The thickness of the laser sheet within the FOV was measured using a fine-scale ruler and was found to be 1.5 mm. The captured images of the flow were processed using LaVision DaVis 10 software package and a NVidia® RTX 2080 graphical processing unit performing temporal correlation calculations. Multi-pass vector calculation was used with an initially larger, 64×64 pixel window size and 50% overlapping followed by a smaller, 16×16 pixel window and 75% overlapping. Two types of data were captured. First, the sampling rate was set to 10,240 frame pairs per second (FPS), and two sets of 10,240 frame pairs were obtained, each corresponding to 1 second of flow time. Next, the sampling rate was set to 1,024 FPS and 10,240 image pairs were captured, corresponding to 10 seconds of data. The former dataset enables a fine temporal flow analysis, while the latter enables the spatial analysis of the flow. In both cases, the dual frames of each image-pair were spaced by 22 microseconds resulting in a particle displacement of 7-8 pixels. From a statistical convergence analysis of Reynolds stresses within the FOV, it was found that 2 seconds of flow data provides a 98% convergence of mean Reynolds stresses.

In general, the wall jet flow passing over the cavity comprises of two major regimes. The lower portion of the flow shows the properties of a zero pressure gradient turbulent boundary layer until a peak value is reached in the velocity profile (U_m). Above the boundary layer, we find a two-dimensional planar shear layer that extends to the quiescent air. The boundary layer thickness (δ , defined from the wall until the maximum velocity in the velocity profile) over the sensor was 13.3 mm, and at this height the velocity magnitude was $U_m = 24$ m/s. The friction Reynolds number (Re_τ), also using the empirical curve-fits of Kleinfelter *et al.* [15], was 990. Additionally, the mean flow structure from the baseline flow was found to be consistent with previous measurements in the same facility as well as existing literature,

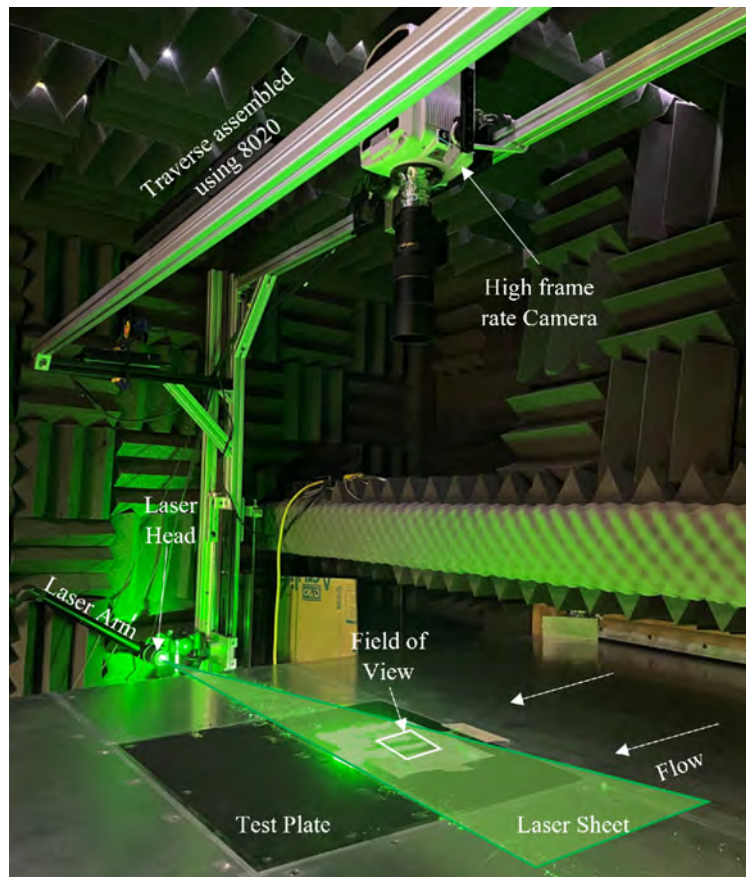


Fig. 9 Wall parallel planar Particle Image Velocimetry (PIV) setup in the wall jet facility at Virginia Tech.

see Szőke [17] for further details. It is worth mentioning that one viscous unit (ν/u_τ) corresponds to 0.0134 mm.

In terms of flow disturbance, we may anticipate the following effects from the cavity on the flow. First, there may be a standing wave in the cavity that acts as an excitation to the flow. Assuming that the cavity interferes with the flow, this effect shall be revealed by the wavenumber-frequency spectrum of the flow that is passing over the cavity. As the flow is homogeneous both in the streamwise and the spanwise directions, this quantity is relatively straight forward to obtain and it is addressed in the following paragraphs. In the case of a constant pressure difference being present over the two sides of the cavity, i.e., below and above the cavity, a bias flow across the cavity would develop. As the flow streamlines are parallel above the plate, the flow was previously shown to be zero-pressure gradient in the wall jet, and as the bottom side of the cavity was situated at the same volume of air as the wall jet flow, we can exclude this concern here. Finally, there may be an interaction between the Kevlar itself and the flow. While direct measurement of this effect is not yet available in the literature, various indirect indications were presented where Kevlar was observed to behave as a no-slip wall when no pressure difference was present on the two sides of the fabric [18, 19], which was also the case here. The reason behind the no-slip behavior of the Kevlar fabric can be understood considering two of its properties, the open area ratio (OAR) and the size of the pores in the fabric. The former is 2% for the Kevlar used here (see fabric K120-EAS in [18]). Additional relevant property of the Kevlar used here is its weave density measured as threads per inch, TPI. Here, TPI was 34 in both the warp and weft directions. The pore size can be calculated from the OAR and TPI, and it is approximately 0.1 mm, which corresponds to 8 viscous units. We can see that the rather small OAR restricts any bias flow to pass through the fabric, while the fine distribution (i.e., 34 pores per inch) and the small pore size (comparable in size to the thickness of the viscous sub-layer) makes flow interactions less likely to exist. Considering the Kevlar from the flow's perspective, it is seen as a 98% solid, no-slip wall.

Figure 10 show maps of the mean flow over the Kevlar interfaced cavity, measured 1.25 mm parallel to the wall. Here the horizontal axis shows the distance along the flow direction and vertical axis is along the span. The streamwise mean velocity is generally $0.85U_m \pm 0.07U_m$ and seems to be unaffected by the cavity, with the values showing no explicit variation across the cavity. The spanwise mean flow (Figure 10b) is almost absent, at less than 1% of U_m , also suggests the negligible effect of the cavity on the mean flow. Similarly, the turbulence statistics, shown in Figure 11 with streamwise turbulent normal stress in 11(a), and spanwise turbulent normal stress in 11(b), showing that the levels are generally uniform at $0.16U_m \pm 0.004U_m$ and $0.15U_m \pm 0.006U_m$ and suggests no apparent influence of the cavity on the turbulence statistics.

Figure 12(a), shows the autospectrum of the streamwise velocity fluctuations at the streamwise location of the cavity centerline ($x_1 = 0$) as a function of frequency and spanwise position (x_3). The autospectral density normalized on the boundary layer timescales (U_m and δ) suggests that the flow is spanwise uniform to within 0.8 dB and, while not shown here, is generally true at all streamwise positions, both upstream and downstream of the cavity. To quantitatively examine any effect of the cavity on the spectral structure of the turbulence, Figure 12(b) shows the line spectrum at the center-span ($x_3 = 0$) at three streamwise locations: the center of the cavity ($x_1 = 0$), upstream of the cavity ($x_1 = -30$ mm) and downstream of the cavity ($x_1 = 30$ mm). The spectra at all stations appear to be consistent to within 2 dB, suggesting the cavity does not seem to interfere at the shown timescales.

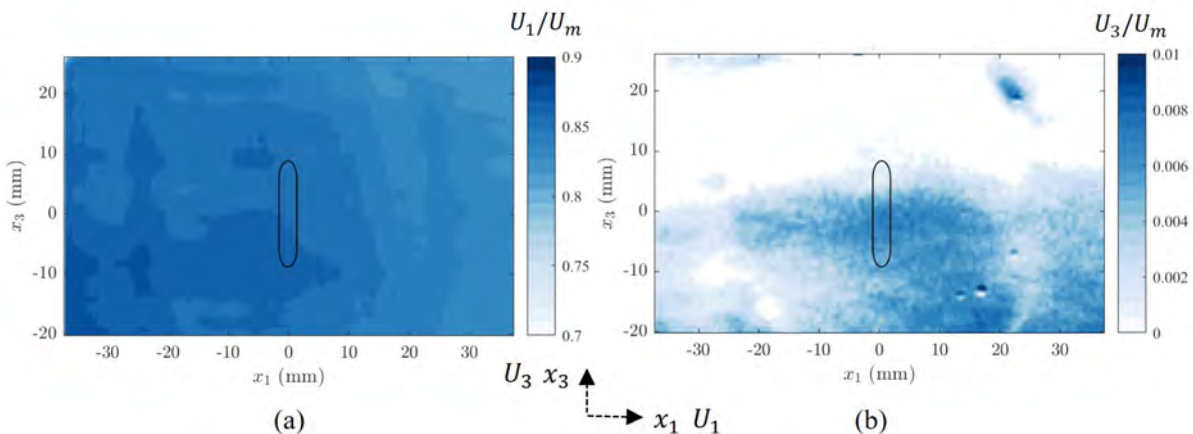


Fig. 10 Mean flow statistics in a wall-parallel plane over the Kevlar interfaced cavity surface

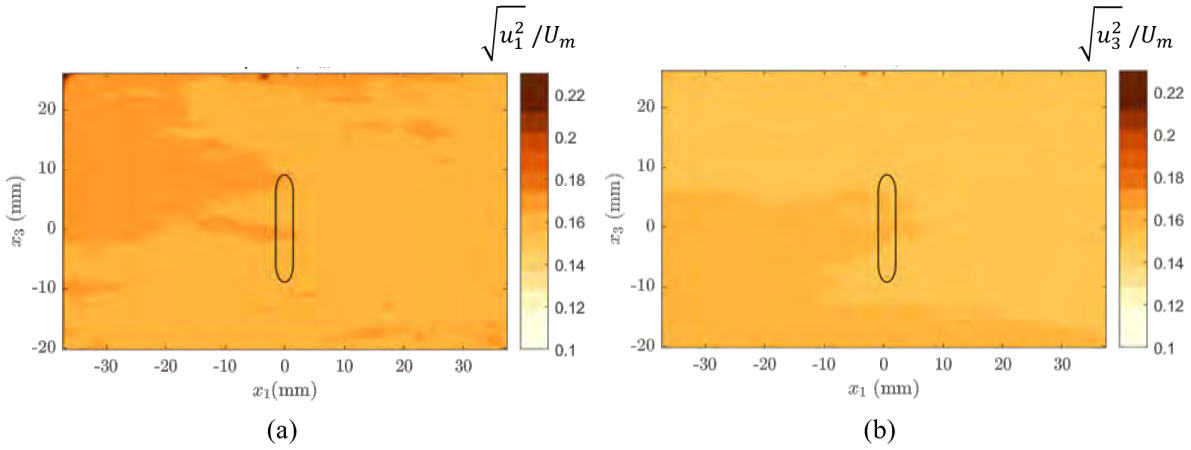


Fig. 11 Turbulence statistics in a wall-parallel plane over the Kevlar interfaced cavity surface

It is possible that the resonator cavity could be weakly withdrawing energy from the flow at spanwise modes consistent with the cavity span. To investigate this possibility we used the measurements to estimate the frequency-wavenumber spectrum $G_{uu}(f, k)$, which decomposes the autospectrum shown in Figure 12(b) as a function of wavenumber. Figure 13(a,b,c) show the frequency-wavenumber spectrum, $G_{uu}(f, k)$, at upstream of the cavity, center of the cavity and downstream of the cavity respectively, the x_1 locations corresponding to the three line spectra Figure 12(b). Contours of the wavenumber spectra, normalized with the boundary layer length and time scales (δ, U_m) suggest that the influence of the cavity on the flow, even at modes corresponding to the cavity span, is within the uncertainty.

In a study by Damani *et al.*[20], examination of the mean flow, Reynolds stresses and the turbulence spectrum in the wall-normal cross-section revealed a negligible effect of the Kevlar interfaced cavity on the flow in a plane aligned with the direction of the wall and passing through a half-wave cavity which was part of an acoustic metasurface. Comparison of the streamwise and wall-normal velocity revealed that the differences between the cavity and the baseline cases were within the measurement uncertainty. While this suggests the limited effect of the cavity in a wall-normal cross-section, an effect, if any, would be apparent in a plane parallel to the cavity surface. It is possible that some turbulent energy is

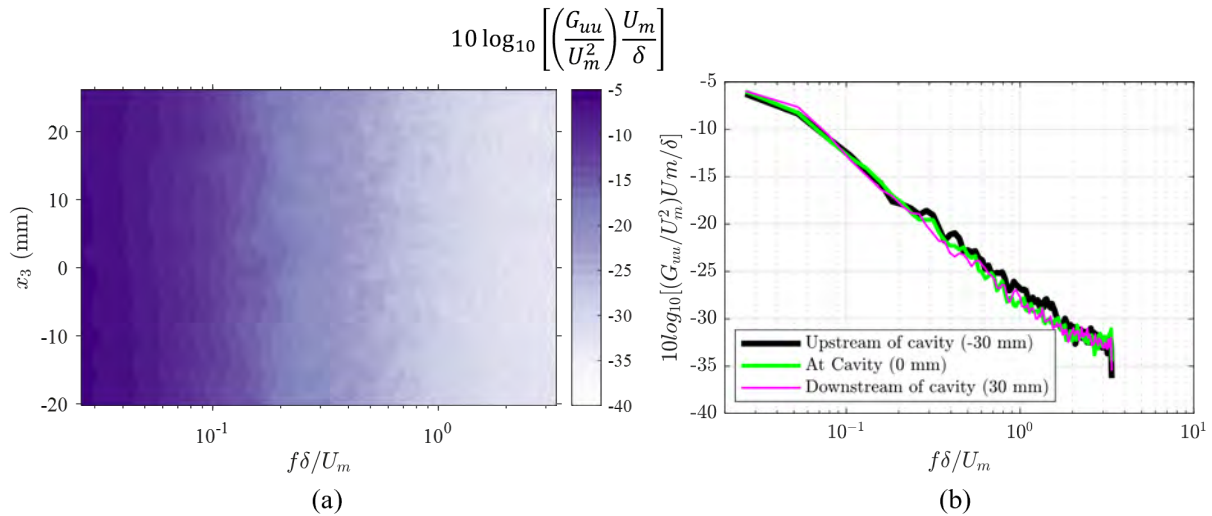


Fig. 12 (a) Contours of the spectrum of the streamwise turbulent velocity shown as along a spanwise line centered over the cavity. (b) Line spectra of the streamwise turbulent velocity upstream of the cavity, over the cavity and downstream of cavity

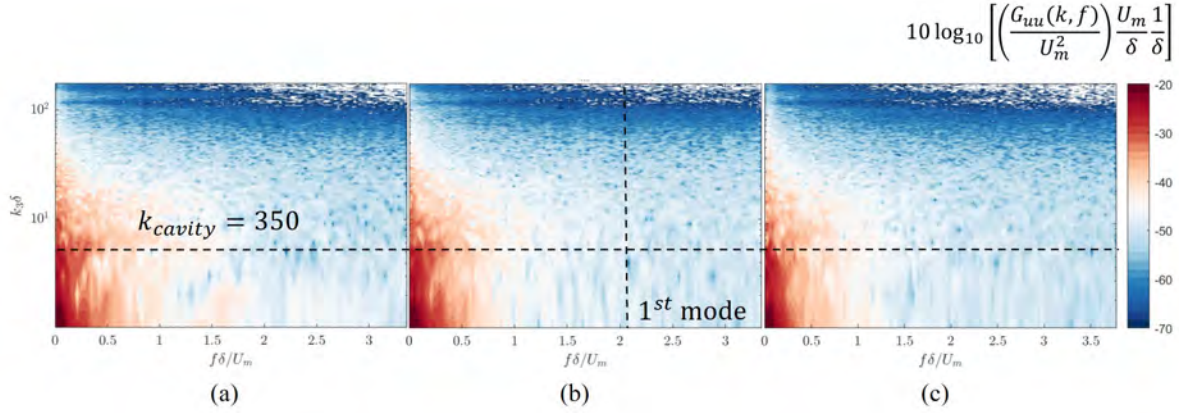


Fig. 13 Frequency-wavenumber spectrum at three locations along the flow direction. (a) Upstream of cavity, (b) Over mid-cavity, (c) Downstream of cavity

transferred towards the excitation of the Kevlar interfaced cavity, particularly around the cavity's resonant frequency. Specifically, it would manifest as a reduction in the energy-spectrum near the wavenumbers corresponding to the cavity size. Alternately, one could also expect the acoustic motions within the cavity to have some feedback on the flow.

These observations and those of the preceding sections clearly suggest that the Kevlar interfaced cavity is a uniformly weighted-area averaging sensor that does not impact the over-riding flow, confirming its suitability for flow-sensing applications, such as the low-wavenumber pressure fluctuations, and the far-field noise. This can be achieved by arranging an array of Kevlar interfaced cavities such that they filter out the strong convective portions of the turbulence, but sufficiently resolve weaker sub-convective portions. This has been demonstrated by the study on low-wavenumber pressure measurements on turbulent boundary layers by Damani [14].

E. Effects of Flow Interface

An additional set of studies were performed to quantify the effects of the characteristics of the flow interface on the behavior of a resonating sensor. The incentive behind this was to have a degree of control over the area sensitivity function of the sensor. Considering a thin material with pores such as the Kevlar scrim, the material can communicate pressure fluctuations due to its flexibility and porosity. If it can be demonstrated that only pores are needed for a sensor to operate satisfactorily, then the spatial sensitivity function could be tailored by customizing the distribution of pores. The flow interface imposes an acoustic impedance boundary condition on the resonating cavity which affects the dynamical properties of the resonating cavity system. The sensor dynamic response function of the sensor with different interfaces was found using the same procedure as described in section III.A. The cavity profile was fixed as the slot (Sensor A) and the flow interface was changed by varying the material, OAR and porosity distribution.

Rigid sheet metal interfaces made of 6061 aluminum were manufactured by precisely drilling holes of 0.36 mm diameter using a CNC machine. An incentive of choosing a rigid material interfaces was to see if the effects of flexibility could be eliminated. Figure 14 shows the pore distribution along with the dimensions of the manufactured interface. The membranes were installed over the surface such that the pore distribution was over the area of the cavity. A specific set of interfaces were chosen to see the effects of material thickness, porosity distribution and open area effects. These cases have been identified in Table 2 which use the same nomenclature as Table 1. Note that sensor type A is a no interface case which acts as a reference case and the 0% OAR case for the aluminum sheet is a blocked sensor case, solid aluminum membrane without any pores. For sensor type J and K, the OAR is the same but the porosity distribution is different. Type J involved blocking the right half of the pores while Type K involved blocking alternate columns of pores as seen in Figure 14(a) using a 40 micron tape. Case B, L and M involve a Kevlar scrim interface of varying OAR. Note that the 0.01% OAR Kevlar interface is a tightly woven sheet of Kevlar with minimal transmission in the presence of no pressure difference between the two sides of the Kevlar.

Figure 15(a) shows the sensor dynamic response function of a slotted cavity when covered by a rigid sheet metal flow interface. The curves have been 12th octave binned and the frequency is cut-off at 10 kHz which corresponds to the spanwise mode of the cavity. The black dashed curve (Sensor A) refers to the no interface case and is shown

| Sensor Type | Material | Thickness (mm) | Modulus(GPa) | OAR(%) | Pore/Weave spacing |
|-------------|---------------|----------------|--------------|--------|----------------------|
| A | None | None | None | 100 | None |
| B | Kevlar 120 | 0.08 | 30 | 2 | 34/34 (filaments/in) |
| G | 6061 Aluminum | 0.508 | 282.7 | 0 | 1.4/0.84 (mm) |
| H | 6061 Aluminum | 0.508 | 282.7 | 6.6 | 1.4/0.84 (mm) |
| I | 6061 Aluminum | 0.406 | 241.3 | 6.6 | 1.4/0.84 (mm) |
| J | 6061 Aluminum | 0.508 | 282.7 | 3.3 | 1.4/0.84 (mm) |
| K | 6061 Aluminum | 0.508 | 282.7 | 3.3 | 2.8/0.84 (mm) |
| L | Kevlar 120 | 0.08 | 30 | 0.01 | 24/73 (filaments/in) |
| M | Kevlar 120 | 0.08 | 30 | 6 | 34/34 (filaments/in) |

Table 2 Table summarizing types of flow interfaces studied using Sensor A

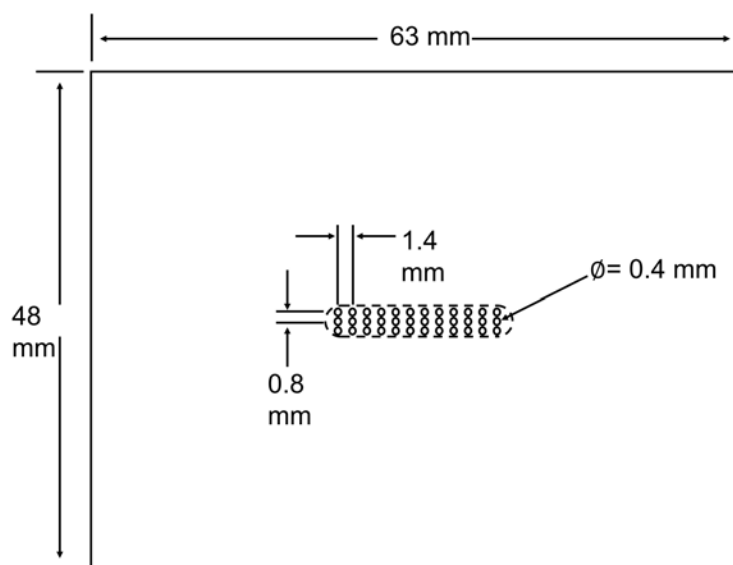


Fig. 14 Dimensions of manufactured rigid sheet metal flow interface. Dashed line represents location of sensor A relative to the pores.

for reference with a resonant depth mode at about 3600 Hz. The blue curve (Sensor G) represents a flow interface made of a sheet metal piece with no pores and excited by a white noise source in the far-field. It is observed that the sensor dynamic response is greatly reduced and likely negligible when fully blocked, the blue curve in Figure 15(a) representing residual uncertainty. Comparing this with sensor H's dynamic response which used the same material as sensor G but had a pore distribution as depicted in Figure 14. The fundamental resonant mode can be identified as the first peak around 2600 Hz and the next harmonic is seen at 9000 Hz. The resonant mode and the harmonic is lower when compared to sensor A due to a change in the cavity acoustic impedance boundary condition by the presence of the flow interface. The same material interface with lesser thickness (sensor I) suggests a slight increase in the frequency of modal response. This result suggests that a resonating sensor can be constructed with a rigid flow interface where pressure excitation from the flow is mediated only by pores in the interface. This raises the possibility that by changing the distribution of pores we can change the spatial sensitivity function.

Hence, the effects of the porosity distribution and open area are studied using sensor types I through M. Figure 15(b) shows the sensor dynamic response function for sensor types involving a difference in their open-area-ratio and porosity distributions. Here, the dashed curve shows the reference case of sensor A. From Figure 15(b), for sensors J and K, it can be seen that the resonant frequency does not change although there is some reduced sensitivity at frequencies above the resonance for sensor J. This indicates that the porosity distribution does have some role in the sensor dynamic

response. Additionally, different open-area-ratio Kevlar scrims were tested to understand the effects of the OAR on the sensor dynamic response with a uniform porosity distribution. From curves corresponding to sensor B, L and M, it can be observed that the change in OAR changes the impedance boundary condition over the sensor which affects the sensor dynamic response which can be calibrated for.

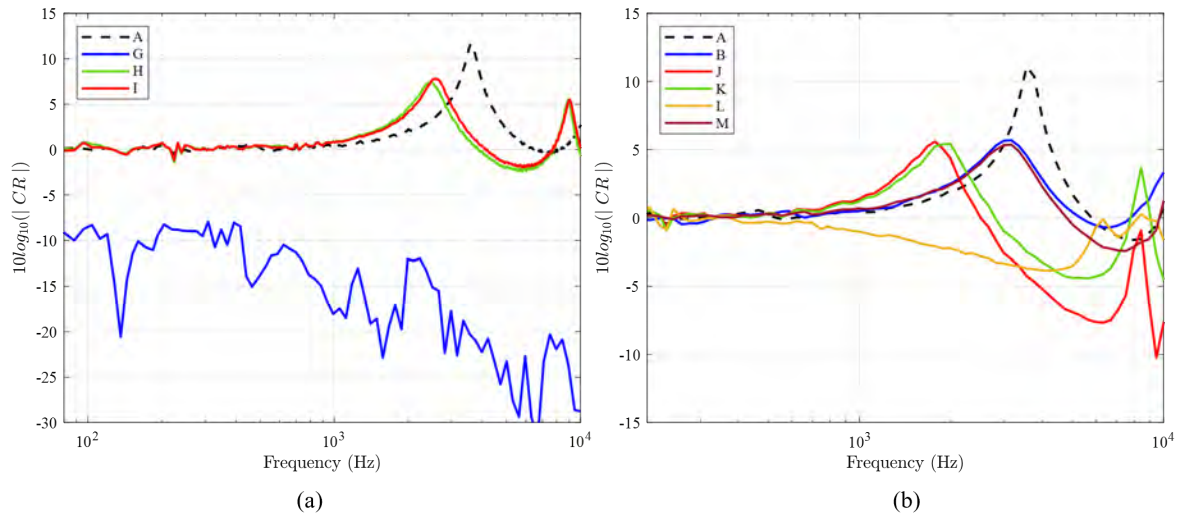


Fig. 15 Sensor dynamic response functions (a) showing effects of material flexibility, (b) showing effects of porosity distribution and OAR

IV. Conclusions

A new type of resonating surface pressure sensor for the measurement of fluctuating pressures over large areas has been studied. These sensors are simple to construct in a wide variety of forms using rapid prototyping and inexpensive transducers. Thirteen different sensor designs were tested in various ways, to examine the influence of shape on the sensor dynamic response and pressure field coherence, to determine the spatial sensitivity function of the sensor, to examine the effects of a Kevlar flow interface upon an over-riding turbulent flow, and to reveal the effects of different interface designs using rigid materials with pores. The following conclusions are drawn:

- 1) The resonator-based cavity sensor offers a degree of freedom using shape, with a sensor dynamic response function which could be calibrated. The sensor dynamic response is limited by the physical dimensions of the cavity especially the fundamental mode associated with the largest dimension of the shape profile. The depth does not play a major role in regard to the functional nature of the sensor.
- 2) A Kevlar-covered acoustic resonator-based cavity has area averaging properties which make it viable as a pressure sensor.
- 3) A Kevlar-covered cavity has negligible effects on the flow rendering the use of such systems in flow applications especially turbulent boundary layer flows.
- 4) The thin flow interface over the resonator-based sensor acts as an impedance boundary condition which changes its dynamic response that could be calibrated for. The type of capping tunes the dynamical properties of the resonating cavity system.
- 5) The interface has no effects due to its flexibility and the sensor dynamic response was shown to be a function of porosity of the interface employed to cap the cavity.
- 6) In general, the sensor dynamic response observes a shift in resonant frequency as the open area changes over the cavity. This is observed due to the change in the dynamical coefficients of the resonator cavity system.
- 7) A change in the porosity distribution with the same open area has secondary effects on the sensor dynamic response of the membrane covered cavity which can be calibrated.

The uniform spatial sensitivity and non-intrusive effects on flow of resonator-based cavity sensors lay the foundation of use of these sensors in flow applications. The degree of freedom obtained from flow interfaces and shapes of cavity

of acoustic resonator-based sensors suggest the use of these sensors for measurements which have been difficult in the past such as detecting low-wavenumber pressure fluctuations in turbulent boundary layer flows. This application particularly takes advantage of the area-averaging and shape of the cavity to sample data in space by averaging over the convective scales and minimize aliasing to capture large-scale structures in flows which are difficult to measure with existing pressure sensor technology. The use of rigid material interface with user-defined porosity distribution in flow applications maybe viable once their influence on the turbulent boundary layer is quantified. This would prove useful for selectively area-averaging in space.

Acknowledgments

The authors would like to thank the Office of Naval Research, in particular Dr. Greg Orris, for their support under grant N00014-21-1-2500. The authors at Exeter would like to thank Dr. John Smith and the Defence, Science and Technology Laboratory (DSTL) for financially supporting this research.

References

- [1] Willmarth, W. W., and Woolridge, C. E., "Measurements of the fluctuating pressure at the wall beneath a thick turbulent boundary layer," *Journal of Fluid Mechanics*, Vol. 14, No. 2, 1962, pp. 187–210. <https://doi.org/10.1017/S0022112062001160>.
- [2] Bull, M., "Wall-pressure fluctuations associated with subsonic turbulent boundary layer flow," *Journal of Fluid Mechanics*, Vol. 28, No. 4, 1967, pp. 719–754. <https://doi.org/10.1017/S0022112067002411>.
- [3] Graham, W. R., "Boundary layer induced noise in aircraft, part I: the flat plate model," *Journal of Sound and Vibration*, Vol. 192, No. 1, 1996, pp. 101–120. <https://doi.org/10.1006/jsvi.1996.0178>.
- [4] Maidanik, G., and Jorgensen, D. W., "Boundary Wave-Vector Filters for the Study of the Pressure Field in a Turbulent Boundary Layer," *Journal of Acoustical Society of America*, Vol. 42, No. 2, 1967, pp. 494–501. <https://doi.org/10.1121/1.1910606>.
- [5] Farabee, T. M., and Geib, F. E. J., "Measurements of Boundary Layer Pressure Fluctuations at Low Wavenumbers on Smooth and Rough Walls," *NCA - Flow Noise Modeling, Measurement, and Control*, 1991.
- [6] Jameson, P. W., "Measurement of the Low-Wavenumber Component of Turbulent Boundary Layer Pressure Spectral Density," *Symposia on Turbulence in Liquids*, 1975.
- [7] K.Bonness, W., E.Capone, D., and A.Hambric, S., "Low-wavenumber turbulent boundary layer wall-pressure measurements from vibration data on a cylinder in pipe flow," *Journal of Sound and Vibration*, Vol. 329, No. 20, 2010, pp. 4166–4180. <https://doi.org/10.1016/j.jsv.2010.04.010>.
- [8] Arguillat, B., Ricot, D., Robert, G., and Bailly, C., "Measurements of the wavenumber-frequency spectrum of wall pressure fluctuations under turbulent flows," *11th AIAA/CEAS Aeroacoustics Conference*, 2005. <https://doi.org/10.2514/6.2005-2855>.
- [9] Ehrenfried, K., and Koop, L., "Pressure Fluctuations Beneath a Compressible Turbulent Boundary Layer," *14th AIAA/CEAS Aeroacoustics Conference*, 2008. <https://doi.org/10.2514/6.2008-2800>.
- [10] Blake, W., "Essentials of Turbulent Wall Pressure Fluctuations," *Mechanics of Flow Induced Sound and Vibration*, Academic Press, Orlando, Florida, 1986.
- [11] Graham, W. R., "A Comparison of Models for the Wavenumber-Frequency Spectrum of Turbulent Boundary Layer Pressures," *Journal of Sound and Vibration*, Vol. 206, No. 4, 1997, pp. 541–565. <https://doi.org/10.1006/jsvi.1997.1114>.
- [12] Gregory, J. W., Sakaue, H., Liu, T., and Sullivan, J. P., "Fast Pressure-Sensitive Paint for Flow and Acoustic Diagnostics," *Annual Review of Fluid Mechanics*, 2013. <https://doi.org/10.1146/annurev-fluid-010313-141304>.
- [13] Damani, S., Alexander, W. N., Devenport, W. J., Pearce, B. P., Shelley, S. R., Starkey, T. A., Hibbins, A. P., and Sambles, J. R., "Excitation of Airborne Acoustic Surface Modes Driven by a Turbulent Flow," *AIAA Journal*, Vol. 59, No. 12, 2021, pp. 5011, 5019. <https://doi.org/10.2514/1.J060662>.
- [14] Damani, S., Butt, H., Banks, J., Srivastava, S., Lowe, T. K., and Devenport, W. J., "Low-Wavenumber Wall Pressure Measurements in Zero-Pressure Gradient Boundary Layer Flow," *AIAA Paper 2022-1795*, 2022. <https://doi.org/10.2514/6.2022-1795>.
- [15] Kleinfelder, A. W., Repasky, R., Hari, N., Letica, S., Vishwanathan, V., Organski, L., Schwaner, J., Alexander, W. N., and Devenport, W. J., "Development and calibration of a new anechoic wall jet wind tunnel," *AIAA Paper 2019-1936*, 2019. <https://doi.org/10.2514/6.2019-1936>.

- [16] Adrian, R. J., and Westerweel, J., *Particle image velocimetry*, 30, Cambridge university press, 2011.
- [17] Szóke, M., Hari, N. N., Devenport, W. J., Glegg, S. A., and Teschner, T. R., "Flow Field Analysis Around Pressure Shielding Structures," *AIAA Paper 2021-2293*, 2021. <https://doi.org/10.2514/6.2021-2293>.
- [18] Szoke, M., Glegg, S. A., and Devenport, W. J., "Investigating the Aeroacoustic Properties of Kevlar Fabrics," *AIAA AVIATION 2021 FORUM*, 2021, p. 2255. <https://doi.org/10.2514/6.2021-2255>.
- [19] Szóke, M., Borgoltz, A., and Devenport, W. J., "Fluid–Structure Interaction Modeling of Flowfields Within Kevlar-Walled Wind Tunnels," *Journal of Aircraft*, 2022, pp. 1–14. <https://doi.org/10.2514/1.C036724>.
- [20] Damani, S., "Excitation of Acoustic Surface Waves by Turbulence," *ETDs*, Virginia Tech, Blacksburg, Virginia, 2021. URL <http://hdl.handle.net/10919/104742>.